ACS OMEGA

http://pubs.acs.org/journal/acsodf

Article

Highly Cross-linked Epoxy Coating for Barring Organophosphate Chemical Warfare Agent Permeation

Guoqing Wu, Dongjiu Zhang, Wei Xu, Hongjun Zhang, Likun Chen, Yongchao Zheng, Yi Xin, Hong Li,* and Yan Cui*

Cite This: *ACS Omega* 2022, 7, 12354−12364

Read Online

ACCESS | Metrics & More | Article Recommendations | Supporting Information

ABSTRACT: Chemical warfare agents (CWAs) can be absorbed in polymeric coatings through absorption and permeation, thus presenting a lethal touch and vapor hazards to people. Developing a highly impermeable polymer coating against CWAs, especially against organophosphate CWAs (OPs), is challenging and desirable. Herein, fluorinated epoxy (F-EP) and epoxy (EP) coatings with different cross-link densities were prepared to resist OPs. The effects of the polymer coating structure, including cross-link density, chemical composition and free volume, on the chemical resistance to dimethyl methylphosphonate (DMMP, Soman simulant) were investigated in detail. Meanwhile, the chemical resistance to Soman and VX was examined. The results reveal that the cross-link density is a critical factor in determining the chemical resistance of the coatings. Highly cross-linked EP and F-EP coatings with dense and solid cross-linked networks can fully bar DMMP and OPs permeation during the test time. At low or medium cross-link densities, the EP coating with a lower retention of DMMP exhibited a higher resistance than the F-EP coating due to the lower interaction with DMMP and smaller free-volume holes and lower relative fractional free volume. These results suggest that increasing the cross-link density is a reasonable approach to control the chemical resistance of polymer networks against OPs.

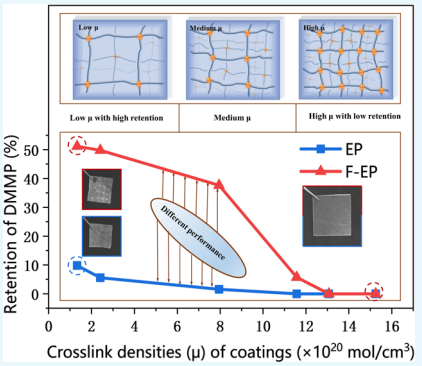

1. INTRODUCTION

Although the usage of chemical warfare agents (CWAs) is explicitly prohibited internationally, the occasional use of CWAs in recent terrorist events provides a reminder that the threat of CWAs still exists.[1−5] CWAs create an immediate threat to creatures upon release, but they also pose a threat via absorption on and permeation into surfaces and could not be decontaminated effectively, creating lethal off-gassing and contact hazards over extended periods of time.[6−10] Polymer coatings in particular, such as those found on vehicles, equipment and buildings, provide a sufficient sink for CWAs uptake.[8−11] So, developing a fully impermeable polymer coating for protection from CWAs is highly desirable.[12−18]

The main reason for the permeation of CWAs into polymer coating can be attributed to the absorption, dissolution and diffusion behaviors of CWAs.[11,19,20] Firstly, like other small molecules, CWAs molecules absorb on the surface of the polymer coating, then gradually permeate into the interior of the polymer due to the thermal movement of the molecules, weakening the interaction force between the macromolecules, and then cause a swelling phenomenon in macroscopic volume expansion.[21−25] In addition, the interaction derived from the physical properties and chemical structure between the CWAs and polymers can also affect the permeation behaviors.[21,26] Organophosphate chemical warfare agents (OPs, nerve agents), such as Soman, VX, and Sarin, are highly toxic organophosphate compounds, which could effectively inhibit acetylcholinesterase (AchE) and lead to nervous system dysfunction. OPs easily spread on the coating surface.[19,27] On the one hand, as a kind of H-bond acceptor, OPs have a strong interaction with many chemical groups such as N−H,[26] the hexafluoroisopropanol (HFIP) group,[28] and other H-bond donors due to H-bond interaction between these groups and phosphate esters.[29] On the other hand, working as a halogen bond (XB) acceptor, the oxygen of the phosphate ester of OPs also has strong interaction with halogens (F, Cl, Br, I) and other XB donors.[30,31] As a result, once they permeate into the polymer coating, it is difficult to decontaminate them. These facts represent a considerable challenge and demand for developing an impermeable polymer coating against OPs. To our knowledge, there are only few reports on protective polymer coating against OPs.[32]

Epoxy resin (EP) is ubiquitously used in various high-performance materials, which is attributed to its ability to form three-dimensional cross-linked networks upon reaction with

Received: February 14, 2022
Accepted: March 22, 2022
Published: March 30, 2022

suitable curing agents.[33] Cross-linking is an effective way to improve the properties of polymers by adjusting their microstructures such as free volume, glass transition temperature, pack density, and the mobility of polymer chains. A properly cross-linked structure determines the properties of the EP polymer such as high mechanical property[34,35] and chemical resistance property.[36,37] For linear polymers, the loosening and untangling of macromolecular chains are caused by swelling, resulting in their being penetrated and dissolved. However, the swelling equilibrium will occur when swelling to a certain extent for cross-linked polymers, and they will not be penetrated and dissolved further.[38,39] The higher the cross-link density, the smaller the degree of swelling when the material reaches the swell equilibrium, and the lower the corresponding permeability. Cross-links are reported to restrict plasticized Brownian motions that assist in fluid uptake behavior.[40]

Herein, fluorinated epoxy (F-EP) and epoxy (EP) coatings with different cross-link densities were prepared by curing a diglycidyl ether of hexafluorobisphenol A and a diglycidyl ether of bisphenol-A with diethylenetriamine (DETA), respectively, and characterized by Fourier transform infrared (FT-IR), NMR, and dynamic mechanical analysis (DMA). The influence of the coating structure on chemical resistance to dimethyl methylphosphonate (DMMP) was investigated in detail by gas chromatography (GC), scanning electron microscopy (SEM), FT-IR, and positron annihilation lifetime spectroscopy (PALS) measurements. The interactions of the F-EP/EP coating surface with DMMP were determined using a quartz crystal microbalance with dissipation monitoring (QCM-D). The protective performance of the prepared polymer coatings against VX and Soman was also examined. The EP and F-EP coatings with a high cross-link density displayed excellent chemical resistance against OPs.

2. MATERIALS AND METHODS

2.1. Chemicals and Materials. Hexafluorobisphenol A (BPAF, 98.0%), epichlorohydrin (ECH, analytical grade), and diethylenetriamine (DETA, 99.0%) were purchased from Aladdin Reagent Co. Ltd. *N*,*N*-Dimethylformamide (DMF, 99.8%) and dimethyl methylphosphonate (DMMP, 98.0%) were obtained from Adamas-β Reagent Co. Ltd. The diglycidyl ether of bisphenol-A type epoxy (DGEBA, E-42) was purchased from Macklin Reagent Co. Ltd. Sodium hydroxide (NaOH, 97.0%) was supplied by Energy Chemical. We bought anhydrous ethanol (EtOH, 99.8%), hydrochloric acid (HCl, 36.0%), acetone (99.5%), and dichloromethane (DCM, 99.5%) from Greagent. Deionized water (H_2O) was fabricated in our lab. All of these reagents were directly used as received without further purification.

2.2. Synthesis and Characterization of DGEFBA. The diglycidyl ether of hexafluorobisphenol A type epoxy (DGEFBA) was prepared by the condensation polymerization of BPAF and ECH. BPAF and ECH were added into a round-bottomed flask (250 mL) at a molar ratio of 1:10, magnetically stirred, and heated to 55 °C within 10 min to completely dissolve the reaction mixture. After adding a little deionized water, 8 g of NaOH was added in four batches. After refluxing at 95 °C for 5 h, the mixture was filtered and rotary evaporated to remove the excess ECH; the obtained light-yellow viscous liquid was dried at 80 °C in vacuum for 12 h, resulting in DGEFBA.

The epoxy value of DGEFBA was determined according to the Chinese standard GB/T 1677−2008 and by the hydrochloric acid-acetone method using eq 1.

$$E = \frac{C(V_0 - V_1)}{10m} \quad (1)$$

where C (mol/L) is the equivalent concentration of the NaOH-EtOH standard solution, V_0 (mL) is the volume of the NaOH-EtOH standard solution consumed in the blank experiments, V_1 (mL) represents the volume of the NaOH-EtOH standard solution consumed in the parallel experiments, and m (g) represents the mass of DGEFBA. The epoxy value of DGEFBA was determined to be 0.40 mol/100 g. DGEBA was purchased from Macklin Reagent Co. Ltd, and its epoxy value was 0.41 mol/100 g.

2.3. Fabrication of F-EP and EP. F-EP coatings with different cross-link densities were obtained by curing of DGEFBA with different amounts of curing agent (DETA), as summarized in Table 1. Firstly, DGEFBA was dissolved in DMF (0.2 g/mL), and DETA was added by stirring. The mixture was then poured into a Teflon mold and cured at 70 °C for 12 h, followed by 100 °C for 2 h to achieve complete curing. After naturally cooling down to room temperature, the coating was peeled off, resulting in F-EP. Using the same procedure, EP coatings with different cross-link densities were prepared by curing of DGEBA with DETA, as summarized in Table 1. The obtained samples were named F-EP90/EP90∼F-EP200/EP200. The number represents the weight of the DETA in the curing reaction.

Table 1. Summary of Mass of DGEFBA and DETA Used for Different Samples

samples	DGEFBA/DGEBA (g)	DETA (mg)
F-EP90/EP90	2	90
F-EP100/EP100	2	100
F-EP120/EP120	2	120
F-EP140/EP140	2	140
F-EP160/EP140	2	160
F-EP200/EP200	2	200

2.4. Chemical Resistance of the Coating to DMMP, Soman, and VX. The chemical resistance of the coating to DMMP was evaluated by measuring the amount of DMMP remaining in and penetrating through the coating. The experiments were performed as follows: three small pieces of filter paper were placed under the peeled coating (0.20 ± 0.05 mm), which were used to absorb DMMP penetrating the coating. Then, DMMP (20 mg) was dropped (see as Figure S1) on the coating surface (2 cm × 2 cm) at 25 °C and a relative humidity of 55%. After 3 h, the surface of the coating was wiped lightly with a cotton ball to remove the remaining DMMP on the surface. Then, the coating and the filter paper were soaked in 10 mL of DCM for 24 h, respectively, and ultrasonicated for 10 min. After filtering, the extraction solvent was analyzed by gas chromatography (GC) to determine the amount of DMMP. The retention of DMMP in the coating and penetration of DMMP through the coating were calculated using eqs 2 and 3.[41]

$$\text{retention}\ (\%) = \frac{W_r}{W_t} \times 100\% \quad (2)$$

https://doi.org/10.1021/acsomega.2c00915
ACS Omega 2022, 7, 12354−12364

Scheme 1. Formation of a Cross-Linked Fluorinated Epoxy Network. (a) Synthesis of DGEFBA from BPAF and ECH; (b) Chemical Reactions between DGEFBA and the Curing Agent DETA

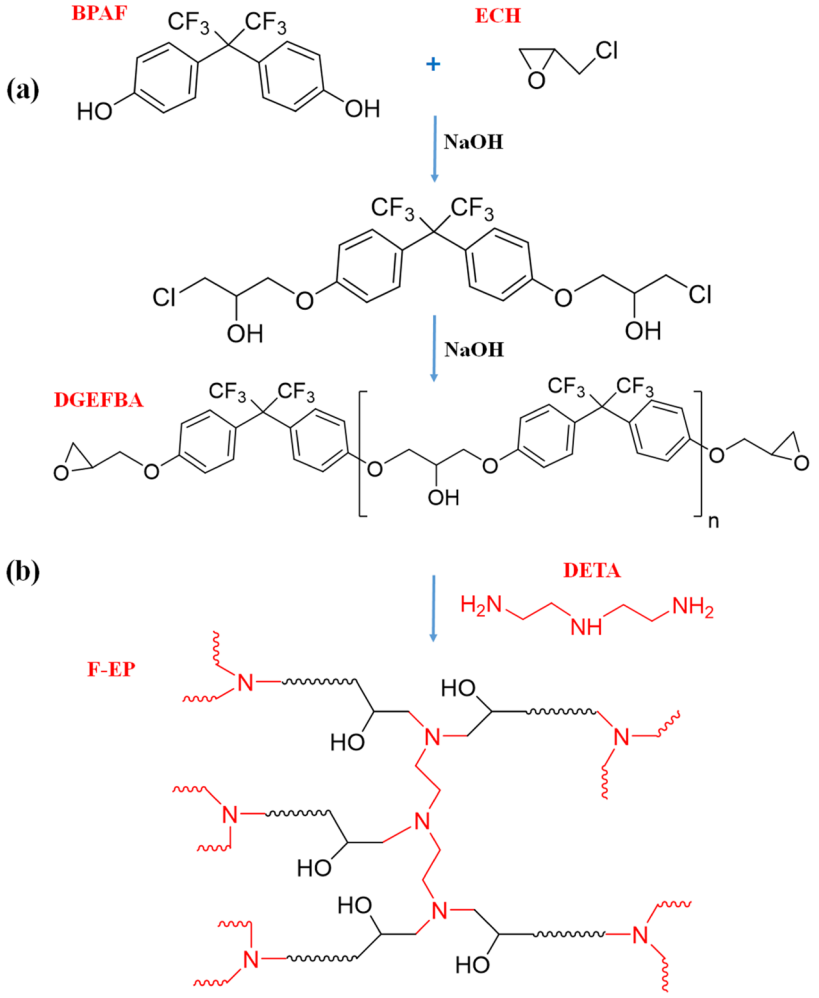

$$\text{penetration}\ (\%) = \frac{W_p}{W_t} \times 100\% \quad (3)$$

where W_t is the total amount of agents (mg) dropped on the coating, W_r is the mass of DMMP (mg) absorbed by the coating, and W_p is the mass of DMMP penetrating through the coating as analyzed by GC. The chemical resistance test of the coating to Soman and VX was conducted using the same procedure, except that the amount of tested Soman and VX dropped on the coating was 1 mg, respectively.

2.5. Characterization. *2.5.1. Dynamic Mechanical Analysis (DMA).* DMA was performed using a dynamic mechanical analyzer (TA Instrument DMA 850) to measure the storage modulus (Ge) and evaluate the cross-link density of the F-EP and EP coatings at a heating rate of 5 °C/min from −10 to 250 °C, a frequency of 1.0 Hz, and a strain amplitude of 0.1%.

2.5.2. Gas Chromatography (GC). GC was performed using Shimadzu GC 2010 to identify the DMMP and then quantitatively analyze it using the standard curve constructed by plotting the DMMP concentrations against their peak area. The tests for Soman and VX were conducted using the same procedure.

2.5.3. Positron Annihilation Lifetime Spectroscopy (PALS) Experiments. PALS experiments were performed using a conventional fast-fast coincidence spectrometer with a time resolution of 210 ps (in FWHM) at 25 °C in air at the University of Science and Technology of China (USTC) to investigate the free volume (V_f) of coatings with different cross-link densities. The positron source prepared by sandwiching the ^{22}Na radioactive source (activity of ∼500 kBq) between two Kapton polyimide foils (10 mm × 10 mm × 7.5 μm) was then sandwiched between two identical samples' stacking of multiple pieces of membranes with a size of 10 mm × 10 mm × 2 mm.

2.5.4. Quartz Crystal Microbalance with Dissipation Monitoring (QCM-D). QCM-D measurements were performed using QSense Pro (Finland/Biolin Scientific AB). The DGEFBA and DGEBA cured with DETA dissolved in DMF (3 mg/mL) were coated by the drop-coating method (20 μL) on the surface of quartz crystal Au electrode sensors (QSX 301, 4.95 ± 0.05 MHz, 14 mm diameter) purchased from Finland/Biolin Scientific AB. Subsequently, the coated sensors were dried at 70 °C for 12 h, followed by 100 °C for 2 h, resulting in a stable coating, and were then placed in the measurement chamber. The fundamental resonant frequency of the quartz crystal and its overtones (n) were excited by applying an AC voltage. The frequency shifts can be monitored by QCM-D because of the piezoelectric effect of a quartz crystal after adsorbing DMMP.[42] The sensors were tested with

https://doi.org/10.1021/acsomega.2c00915
ACS Omega 2022, 7, 12354−12364

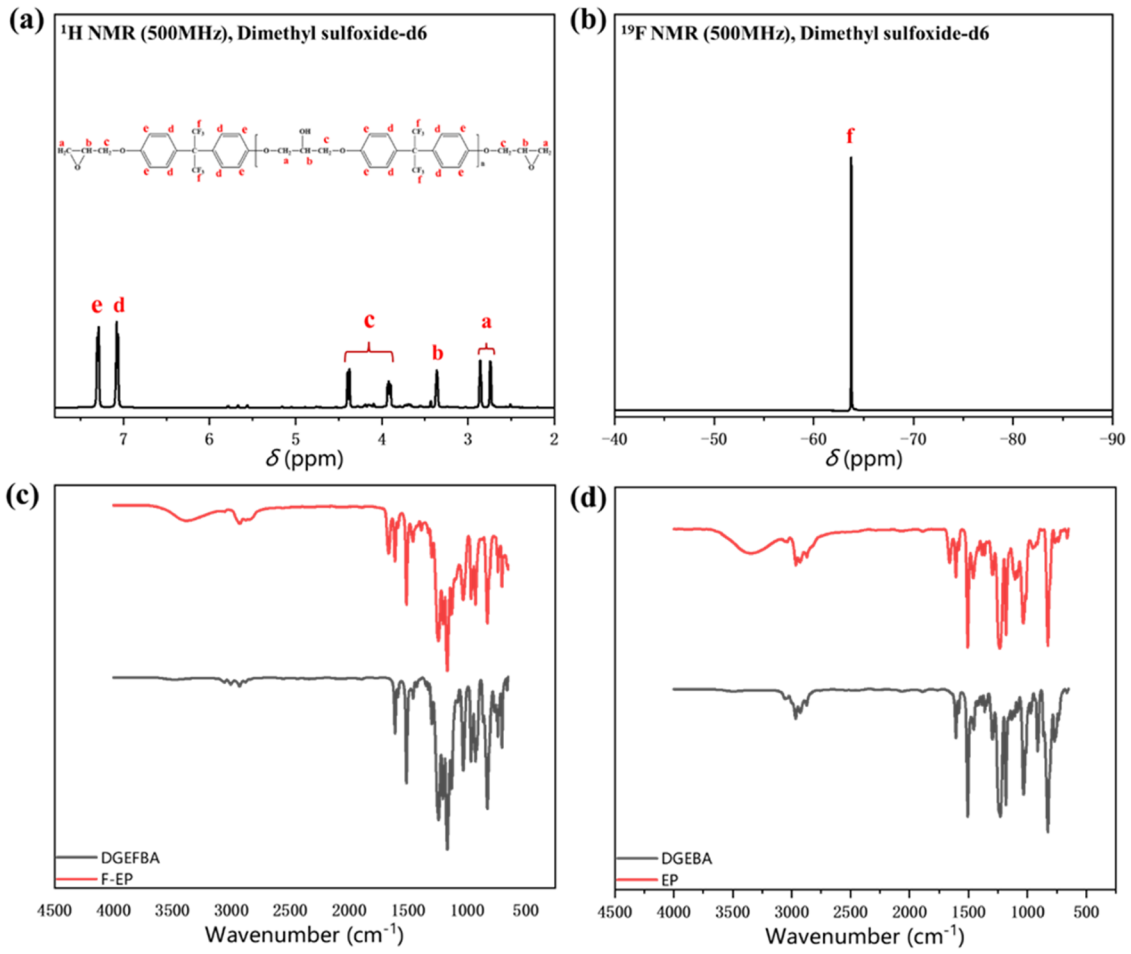

Figure 1. (a) ^{1}H NMR and (b) ^{19}F NMR spectra of DGEFBA; FT-IR spectra of (c) DGEFBA, F-EP and (d) DGEBA, EP.

DMMP at 25 °C and a flow rate of 100 μL/min, while DMMP adsorption was measured after the establishment of a stable baseline.

2.5.5. Other Characterizations. The ^{1}H and ^{19}F NMR of DGEFBA and DGEBA were carried out using Bruker 500 NMR (AVANCE III HD 500). Fourier transform infrared (FT-IR) spectrometry of the coatings in the scanning range of 4000−650 cm^{-1} was characterized using Spectrum 100 (Perkin Elmer). Using the sessile drop method, the contact angles (CA) of the coatings with the liquid were determined using a DSA-30 (Kruss Company) optical contact-angle device by injecting 5 μL of DMMP onto the coatings at 25 °C. The surface and cross-sectional SEM images of the membranes before and after being contaminated were taken using a field emission scanning electron microscope (Nova NanoSEM 450).

3. RESULTS AND DISCUSSION

3.1. Synthesis of F-EP and EP with Different Cross-link Densities. The cross-linked fluorinated epoxy network (F-EP) was synthesized by two steps as shown in Scheme 1. The first one is the synthesis of the fluorinated epoxy resin DGEFBA, followed by curing of DGEFBA with the curing agent of an aliphatic triamine (DETA). DETA was chosen due to its relatively low curing temperature and the ability of reaching high cross-link densities. DGEFBA was characterized by ^{1}H NMR (Figure 1a),^{19}F NMR (Figure 1b), and FT-IR (Figure 1c). The ^{1}H NMR peaks of DGEFBA at 2.86 and 2.74 ppm in Figure 1a were attributed to the two hydrogens of the methylene group on the epoxy group, and the peak at 3.36 ppm was assigned to the methine hydrogen on the epoxy group. The chemical shifts of the two hydrogens on the methylene group adjacent to the epoxy group were at 3.92 and 4.38 ppm, respectively, and the chemical shifts at 7.29 and 7.08 ppm were attributed to the adjacent proton peaks on the two aromatic rings. The ^{19}F NMR peak of −63.76 ppm was attributed to trifluoromethyl (−CF_3). The characteristic IR band of DGEFBA at 915 cm^{-1} was clearly observed as shown in Figure 1c, which can be attributed to the stretching vibration of the epoxy group, while the peak intensity was significantly weakened after curing. Moreover, an obvious hydroxyl stretching vibration peak appeared at 3400 cm^{-1} after curing, and the band of C-N between 3300 and 3500 cm^{-1} coincided with the hydroxyl peak. The above results confirmed that the F-EP was successfully prepared. The EP analogue was prepared by curing of commercial DGEBA with DETA, and was characterized by FT-IR (Figure 1d). The FT-IR spectrum of EP is almost the same as that of F-EP, except for the −CF_3 peak at 1100−1200 cm^{-1}.

The cross-link density can be obtained based on the standard rubber elasticity theory, which assumes that the van der Waals and other interactions between molecules have been broken above the glass transition temperature (T_g) and the storage modulus (Ge) is proportional to the number of cross-links present in the network.[43] In this study, the cross-link density was assessed by determining the number average

https://doi.org/10.1021/acsomega.2c00915
ACS Omega 2022, 7, 12354−12364

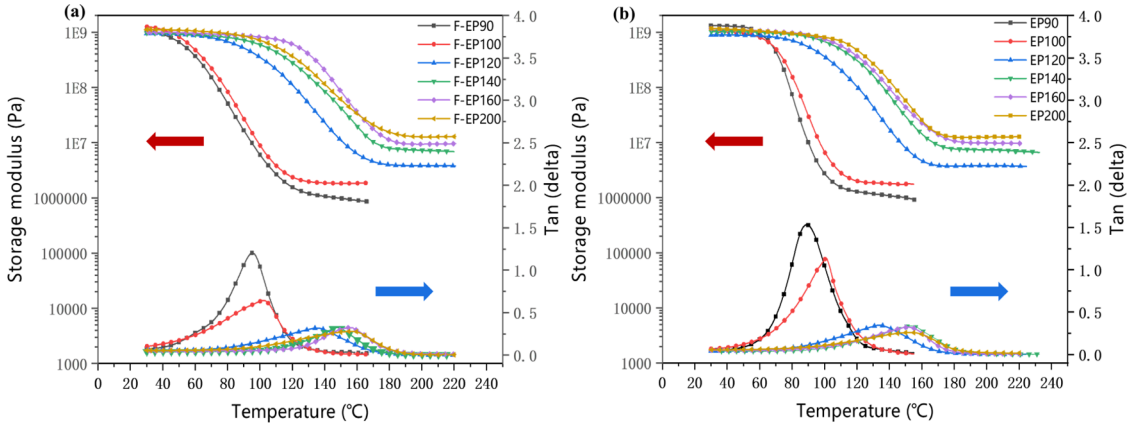

Figure 2. DMA test curves of (a) F-EP and (b) EP.

Table 2. Ge, Mc, μ and T_g Values of F-EP and EP

samples	Ge (MPa)	Mc (g/mol)	$\mu \times 10^{20}$ (mol/cm^3)	T_g (°C)
F-EP90/EP90	1.2/1.2	3023/3023	1.3/1.3	95/90
F-EP100/EP100	1.5/1.5	1664/1664	2.4/2.4	103/100
F-EP120/EP120	3.9/3.8	495/505	8.1/8.0	136/133
F-EP140/EP140	7.2/7.0	341/347	11.8/11.6	146/144
F-EP160/EP160	10.0/9.0	293/307	13.7/13.1	155/152
F-EP200/EP200	14.0/13.0	255/263	15.7/15.3	158/153

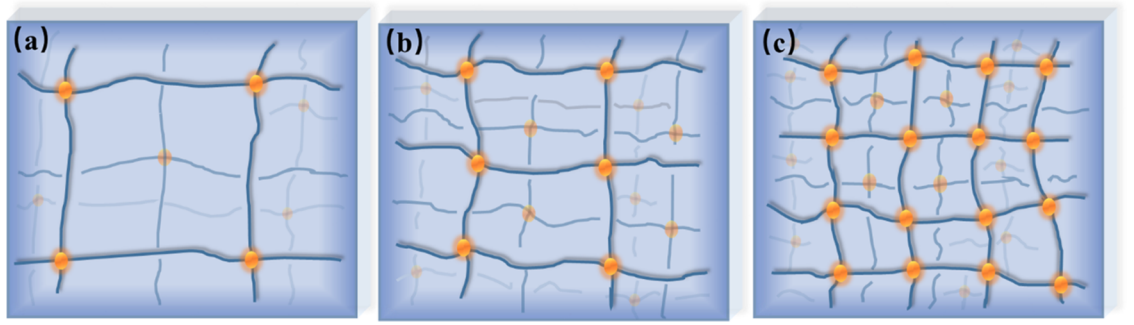

Figure 3. Simplified schematic of F-EP or EP networks for different cross-link densities. (a)−(c) correspond to low, medium, and high cross-link densities respectively.

molecular weight between the cross-links (Mc), which is inversely proportional to μ and can be calculated by Ge using eq 4.[44,45]

$$\log_{10} \mathrm{Ge} = 6.0 + \frac{293\rho}{\mathrm{Mc}} \tag{4}$$

where ρ (g/cm^3) represents the epoxy density and Ge is the rubber storage modulus in the DMA test. Then, the cross-link density (μ) was estimated empirically using eq 5, in which N (6.02×10^{23}) represents Avogadro's number[44]

$$\mu = \frac{\rho N}{1.5\mathrm{Mc}} \tag{5}$$

Figure 2a shows the DMA test curves of the F-EP coatings prepared by using six different amounts of the curing agent DETA. As shown in Figure 2, the glass transition of each sample can be seen in the peak of the tan (delta) plots with temperature, and the polymer transits from the rigid glass state to the flexible rubbery state. The DMA curves gradually decrease from a high storage modulus to the rubber plateau with a low storage modulus (Ge value). With the increase of the cross-link density, the molecular chains are connected into a dense three-dimensional network, which restricts the movement of the molecular chains, resulting in the increase of Ge and T_g. The Ge, T_g, Mc, and μ values calculated from eqs 4 and 5 for the six F-EP coatings are summarized in Table 2. When the amount of DETA increased from 90 to 200 mg, the cross-link density increased about 12 times from 1.3×10^{20} to 15.7×10^{20} mol/cm^3, and the T_g of the coatings increased from 95 to 158 °C, indicating the formation of very dense and solid cross-linking networks. Meanwhile, the Ge, Mc, μ, and T_g values of the EP coatings were determined and calculated by the same method (Figure 2b and Table 2). As shown in Table 2, when the dosage of DETA for EP is the same as that for F-EP, the cross-link density and T_g of EP are basically the same as those of F-EP. Consequently, based on the above results, the simplified schematic for the three kinds of F-EP and EP cross-link networks with low, medium, and high cross-link densities are shown in Figure 3.

3.2. Chemical Resistance of F-EP or EP Coatings to DMMP, VX, and Soman. Firstly, the chemical resistance of F-EP or EP coatings to DMMP is qualitatively evaluated. The

https://doi.org/10.1021/acsomega.2c00915
ACS Omega 2022, 7, 12354−12364

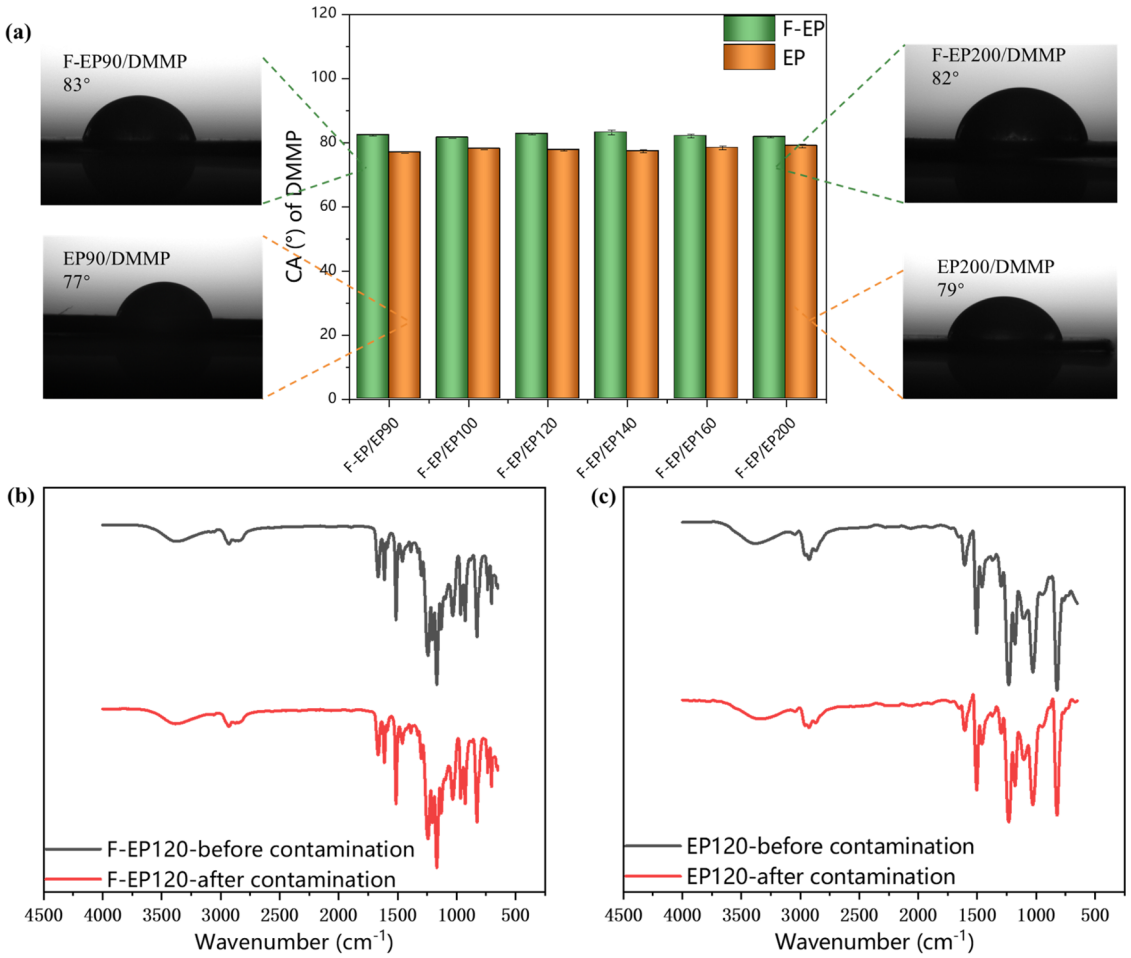

Figure 4. (a) Contact angle (CA) for DMMP on F-EP and EP by injecting 5 μL of DMMP onto the coatings at 25 °C; FT-IR spectra of (b) F-EP120 and (c) EP120 before and after contamination by DMMP.

wettability of DMMP can influence its adsorption on the coating surface. Figure 4a shows the contact angle (CA) of DMMP on the F-EP and EP coatings. All CAs of DMMP on the F-EP and EP coatings are less than 90°, indicating that DMMP wets and spreads on the F-EP and EP surfaces. Probably due to the CF_3 groups in F-EP, the DMMP CAs on F-EP are slightly higher than those on the EP coatings. Figure 4b,c represents the FT-IR spectra of F-EP120 and EP120 before and after contamination by DMMP, respectively. Before the FT-IR test, the coatings after contamination by DMMP were placed in a 70 °C oven for 12 h to remove the completely residual DMMP. There was no obvious peak change in the spectra, which indicated that no chemical reaction happened between the coatings and DMMP. Figure 5 displays the pictures of the F-EP and EP before and after contamination by DMMP for 3 h taken by a digital camera. There is obvious deformation and swelling for F-EP100 and EP100. However, as the cross-link densities of the F-EP and EP coatings increased, no deformation and swelling were observed for the other F-EP/EP samples. Moreover, the surface and cross-sectional SEM images (Figure S2) of all of the samples revealed that there were no conspicuous destructions such as holes for the coatings after being contaminated by DMMP.

Furthermore, the chemical resistance of F-EP and EP coatings to DMMP was quantitatively evaluated for the DMMP remaining in the coatings and penetrating through the coatings. As shown in Figure 6a,b, both F-EP and EP demonstrated excellent chemical resistance to DMMP. No DMMP penetrated through the coatings within 3 h. The retention of the DMMP in the coatings gradually decreased to zero when the cross-link density of the coatings increased to 13.7×10^{20} mol/cm^3 for F-EP160 and 11.6×10^{20} mol/cm^3 for EP140. It means that the F-EP and EP coatings with relatively high cross-link densities are able to completely bar the DMMP during the test time. The dense and solid cross-linked networks fully restrict DMMP from permeating and penetrating the polymer coatings. At low and medium cross-link densities, EP exhibited much lower retention of DMMP than F-EP with the same cross-link density. When the cross-link density was 1.33×10^{20} mol/cm^3, the retention of DMMP in F-EP90 was 51.14%, while the DMMP retention in EP90 was only 9.84%. Also, when the retention of DMMP in EP140 with a cross-link density of 11.6×10^{20} mol/cm^3 reduced to zero, there was still 5.74% DMMP in the F-EP140. The reasons will be discussed later.

We further explored the kinetic plots of DMMP permeation in F-EP and EP. As shown in Figure 6c,d, for F-EP200, EP140, and EP200, no DMMP permeated into the coatings during the test time of 3 h. For F-EP140, DMMP started to permeate into the coating after 2 h. As for F-EP100, 25% of the DMMP permeated into the coating after 0.5 h, and the retention further increased to 30% after 2 h, then quickly rose to 51% after 3 h. The trend of DMMP retention in EP100 with the contaminated time is similar to that of F-EP100, but with a

https://doi.org/10.1021/acsomega.2c00915
ACS Omega 2022, 7, 12354−12364

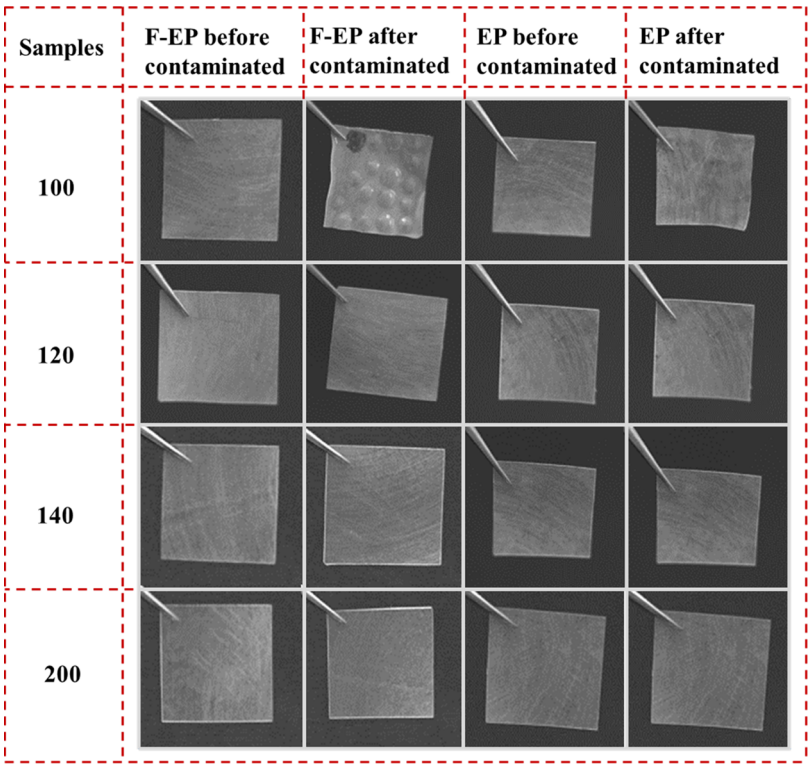

Figure 5. Pictures of F-EP and EP before and after contamination by DMMP for 3 h taken by a digital camera.

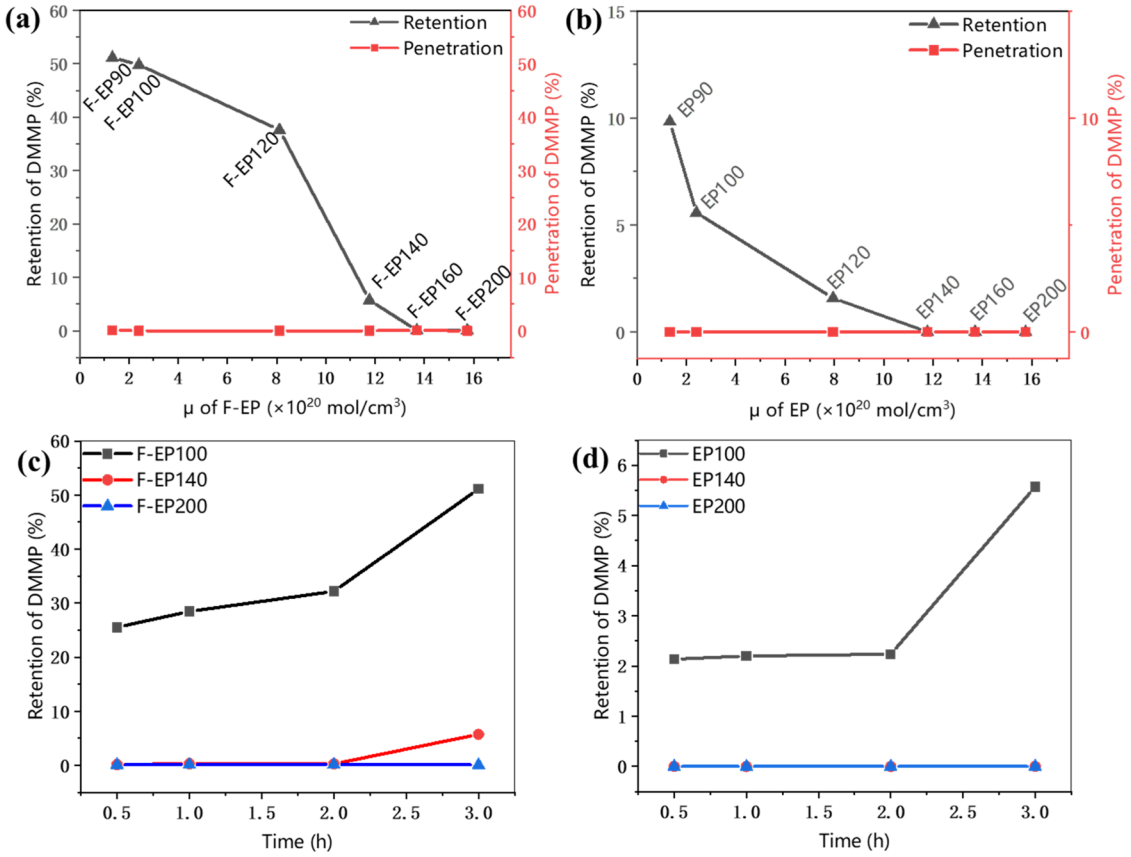

Figure 6. Retention and penetration of DMMP to (a) F-EP and (b) EP with different cross-link densities. Retention and penetration of DMMP to (c) F-EP and (d) EP after being contaminated for different hours at 25 °C and a relative humidity of 55%. The thickness of the coatings was 0.20 ± 0.05 mm.

https://doi.org/10.1021/acsomega.2c00915
ACS Omega 2022, 7, 12354−12364

much lower retention value. DMMP can easily ingress into the F-EP and EP coatings at low cross-link densities and then swell the coatings, which further caused the quick increase of the permeability rate with time. However, the highly cross-linked coatings (F-EP200 and EP200) were able to resist the DMMP completely during the test time. The cross-link density of the coatings is thus a key factor that affects the chemical resistance to DMMP.

In order to verify the protective performance of the coating against real OPs, the chemical resistance values of F-EP200 and EP200 to VX and Soman were calculated and are listed in Table 3. Neither retention nor penetration of VX and Soman was detected by GC after the coatings were contaminated for 24 h, which revealed the excellent protective performance of the highly cross-linked F-EP/EP coatings.

Table 3. Chemical Resistance of F-EP and EP Coating to VX and Soman

	Soman		VX	
	retention (%)	penetration (%)	retention (%)	penetration (%)
F-EP200	not detected	not detected	not detected	not detected
EP200	not detected	not detected	not detected	not detected

3.3. Free Volume of F-EP and EP. Free volume is obtained from the nanoscaled holes randomly distributed in glassy polymers, and it has an important influence on the impermeability of the polymers.[46] Reducing the free-volume hole size is an approach to control the solvent properties for EP networks.[47] Herein, positron annihilation lifetime spectroscopy (PALS) was performed to evaluate the size of the free-volume holes of the polymer coatings.[48] PALS data was analyzed using the LTv9 program, and all spectra were divided into different lifetime components ($\tau_1 < \tau_2 < \tau_3$). The longest lifetime component τ_3 generally corresponds to the pick-off annihilation of *ortho*-positronium (*o*-Ps), which provides information about the size of the free-volume holes.[49] The average radius (R) of the holes was estimated by a semi-empirical equation according to a spherical infinite potential well model[50]

$$\tau_3 = \frac{1}{2}\left[1 - \frac{R}{\Delta R + R} + \left(\frac{1}{2\pi}\right)\sin\left(\frac{2\pi R}{R + \Delta R}\right)\right]^{-1} \quad (6)$$

where ΔR (0.1656 nm) is an empirical parameter of the thickness of the electron layer. The average free volume (V_f) of the holes was calculated by

$$V_f = \frac{4}{3}\pi R^3 \quad (7)$$

The relative fractional free volume (f_r, %) was calculated empirically using eq 8,[48] where the intensity (I_3) corresponded to τ_3 and reflected the number of V_f holes.

$$f_r = V_f I_3 \quad (8)$$

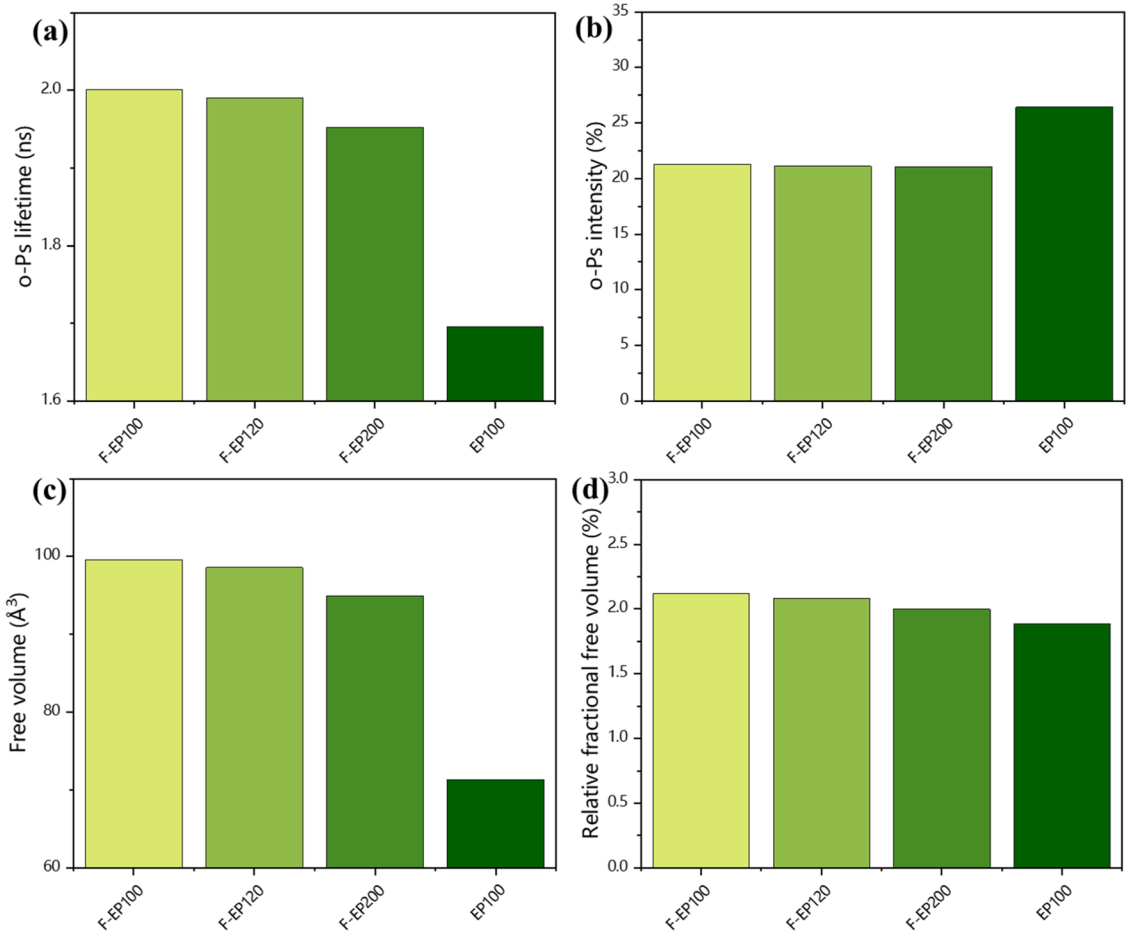

Figure 7. (a) *o*-Ps lifetime, (b) *o*-Ps intensities, (c) free volume, and (d) relative fractional free volume of the F-EP coatings.

https://doi.org/10.1021/acsomega.2c00915
ACS Omega 2022, 7, 12354−12364

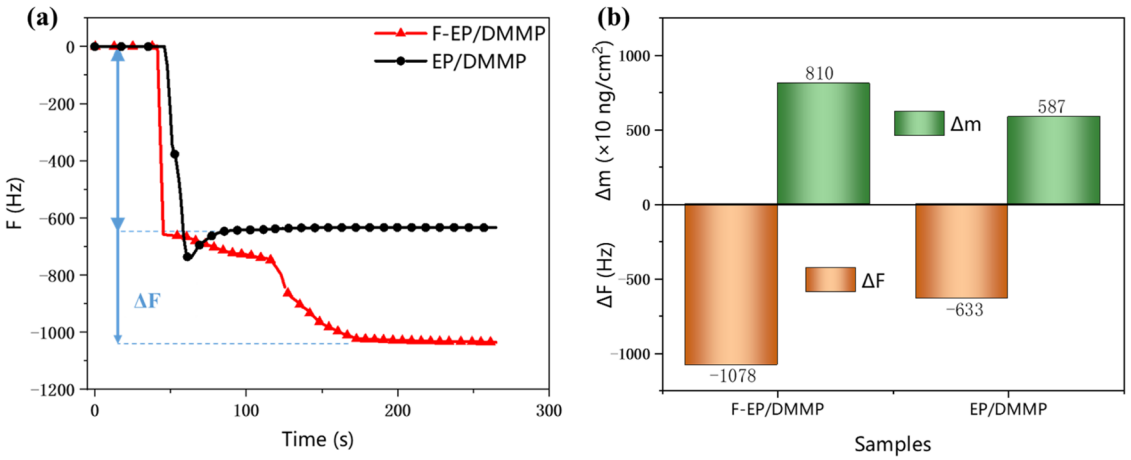

Figure 8. (a) QCM-D response curves for DMMP adsorption on the F-EP- and EP-coated quartz crystal surface; (b) mass changes of sensors (Δm) and QCM-D frequency shifts (ΔF) for DMMP adsorption on F-EP and EP.

Figure 7a,b shows the τ_3 and I_3 of low, medium, and high cross-linked F-EP samples, while V_f and f_r are displayed in Figure 7c,d. The V_f of the F-EP samples ranged from 90 to 100 Å^3 and slightly decreased with the cross-link density. All of the V_f values of the samples are smaller than the calculated van der waals volumes (vdW volume) of DMMP (106 Å^3), Soman (171 Å^3), and VX (261 Å^3). A lower V_f would create a statistically lower probability of chemical transport. The coating with a higher cross-link density will have a lower V_f and higher T_g and rigidity, which would lead to enhanced resistance against DMMP. However, DMMP still can permeate into the low and medium cross-linked coatings even if the coatings have smaller free-volume hole sizes than the calculated vdW volumes of DMMP, as shown in Figure 6. This is probably because the V_f obtained by PALS is an average value. There are some big free-volume holes in the coating that cannot bar DMMP permeation. Once DMMP enters the coating, it further swells the coating, enlarges the free-volume holes, and then causes a quick increase of permeability. On the other hand, EP100 exhibited a much smaller V_f and a slightly lower f_r than F-EP100, indicating that the macromolecular chains of EP100 without the $-CF_3$ groups are arranged much more closely, which should contribute to the improved chemical resistance of EP100 to DMMP than F-EP100.

3.4. Interaction between DMMP and F-EP/EP.

Furthermore, the physical interaction of the F-EP and EP surfaces with DMMP was investigated by QCM-D measurements. By monitoring the change of crystal oscillation frequency (F, Hz), the adsorption characteristics of DMMP on the F-EP and EP surfaces were investigated. According to Sauerbrey equation[51] (eq 9), the negative-frequency changes are proportional to the adsorption mass deposited (Δm)

$$\Delta m = \frac{-C \times \Delta F_n}{n} \quad (9)$$

where C represents the mass sensitivity constant (C = 17.7 ng·cm^{-2}·Hz^{-1} for a 5 MHz crystal sensor[52]) and ΔF_n represents the frequency shift of the nth overtone. As shown in Figure 8a, a negative F with a sharp drop was observed, implying the mass deposition (Figure 8b) of DMMP onto the F-EP/EP-coated sensor. Compared to EP, the higher ΔF_n and Δm of the F-EP-coated sensor at adsorption equilibrium revealed that there existed a stronger physical interaction between the F-EP surface and DMMP. It is known that DMMP is a good halogen bond acceptor due to the chemical portion of −P═O and −P−O− bonds.[26] There may exist a halogen bond[31] interaction between the trifluoromethyl group ($-CF_3$) and phosphate esters, probably resulting in a stronger interaction and higher adsorption between DMMP and F-EP. So, because of the lower free-volume hole size and weaker physical interaction with DMMP, EP has an advantage as a polymer coating material resistant to organophosphate compounds over F-EP.

4. CONCLUSIONS

The fundamental understanding of the relationship between the structure and anti-OPs property of an epoxy coating has been preliminarily established by varying the cross-link density of epoxy and fluorinated epoxy analogues. The results demonstrated that the anti-CWAs performances of the coatings have a strong dependence on their cross-link density. Highly cross-linked EP and F-EP coatings with dense and solid cross-linked networks can completely bar the DMMP simulant and OPs permeation during the test time. At low or medium cross-link densities, the DMMP gradually ingresses into the coatings even if the coatings have smaller free volume than the van der waals volume of DMMP. Due to a weaker interaction with DMMP, smaller free-volume holes, and a relatively fractional free volume, the EP coating exhibited a higher resistance to DMMP than the F-EP coating. These results may play a constructive role in the design and preparation of highly protective coatings against OPs.

■ ASSOCIATED CONTENT

Supporting Information

The Supporting Information is available free of charge at https://pubs.acs.org/doi/10.1021/acsomega.2c00915.

Picture of F-EP contaminated by DMMP (Figure S1); surface SEM and cross-sectional SEM (the inset) images of F-EP and EP coatings before and after contaminated by DMMP for 3 h (Figure S2) (PDF)

■ AUTHOR INFORMATION

Corresponding Authors

Hong Li − *School of Chemistry and Chemical Engineering, Frontiers Science Center for Transformative Molecules, Shanghai Key Lab of Electrical Insulation and Thermal*

https://doi.org/10.1021/acsomega.2c00915
ACS Omega 2022, 7, 12354−12364

Aging, Shanghai Jiao Tong University, Shanghai 200240, P. R. China; orcid.org/0000-0002-0983-4410; Email: lh102@sjtu.edu.cn

Yan Cui − *State Key Laboratory of NBC Protection for Civilian, Beijing 102205, P. R. China; Research Institute of Chemical Defense, Beijing 102205, P. R. China;* Email: tracypiscescy@163.com

Authors

Guoqing Wu − *School of Chemistry and Chemical Engineering, Frontiers Science Center for Transformative Molecules, Shanghai Key Lab of Electrical Insulation and Thermal Aging, Shanghai Jiao Tong University, Shanghai 200240, P. R. China*

Dongjiu Zhang − *School of Chemistry and Chemical Engineering, Frontiers Science Center for Transformative Molecules, Shanghai Key Lab of Electrical Insulation and Thermal Aging, Shanghai Jiao Tong University, Shanghai 200240, P. R. China*

Wei Xu − *State Key Laboratory of Particle Detection and Electronics, University of Science and Technology of China, Hefei 230026, P. R. China*

Hongjun Zhang − *State Key Laboratory of Particle Detection and Electronics, University of Science and Technology of China, Hefei 230026, P. R. China;* orcid.org/0000-0002-4714-8809

Likun Chen − *State Key Laboratory of NBC Protection for Civilian, Beijing 102205, P. R. China; Research Institute of Chemical Defense, Beijing 102205, P. R. China*

Yongchao Zheng − *State Key Laboratory of NBC Protection for Civilian, Beijing 102205, P. R. China; Research Institute of Chemical Defense, Beijing 102205, P. R. China;* orcid.org/0000-0001-9627-5882

Yi Xin − *State Key Laboratory of NBC Protection for Civilian, Beijing 102205, P. R. China; Research Institute of Chemical Defense, Beijing 102205, P. R. China*

Complete contact information is available at: https://pubs.acs.org/10.1021/acsomega.2c00915

Notes

The authors declare no competing financial interest.

■ ACKNOWLEDGMENTS

We appreciate the financial support provided by National Key R&D Program of China (Nos. 2020YFB1505500 and 2020YFB1505502). We gratefully acknowledge funding for this work provided by Pre-research Project 30110020402.The authors thank Instruments Analysis Center of Shanghai Jiao Tong University for GC and SEM measurements and ShanghaiTech University for QCM-D measurements.

■ REFERENCES

(1) Trotochaud, L.; Tsyshevsky, R.; Holdren, S.; Fears, K.; Head, A. R.; Yu, Y.; Karslıoğlu, O.; Pletincx, S.; Eichhorn, B.; Owrutsky, J.; et al. Spectroscopic and Computational Investigation of Room-Temperature Decomposition of a Chemical Warfare Agent Simulant on Polycrystalline Cupric Oxide. *Chem. Mater.* **2017**, *29*, 7483−7496.

(2) Sengele, A.; Robert, D.; Keller, N.; Keller, V.; Herissan, A.; Colbeau-Justin, C. Ta-doped TiO_2 as photocatalyst for UV-A activated elimination of chemical warfare agent simulant. *J. Catal.* **2016**, *334*, 129−141.

(3) Lafuente, M.; Sanz, D.; Urbiztondo, M.; Santamaria, J.; Pina, M. P.; Mallada, R. Gas phase detection of chemical warfare agents CWAs with portable Raman. *J. Hazard. Mater.* **2020**, *384*, No. 121279.

(4) Khan, M. S. J.; Wang, Y. W.; Senge, M. O.; Peng, Y. Sensitive fluorescence on-off probes for the fast detection of a chemical warfare agent mimic. *J. Hazard. Mater.* **2018**, *342*, 10−19.

(5) Chai, X.; Cui, Y.; Xu, W.; Kong, L.; Zuo, Y.; Yuan, L.; Chen, W. Degradation of malathion in the solution of acetyl peroxyborate activated by carbonate: Products, kinetics and mechanism. *J. Hazard. Mater.* **2021**, *407*, No. 124808.

(6) Thiermann, H.; Worek, F.; Kehe, K. Limitations and challenges in treatment of acute chemical warfare agent poisoning. *Chem. Biol. Interact.* **2013**, *206*, 435−443.

(7) Lavoie, J.; Srinivasan, S.; Nagarajan, R. Using cheminformatics to find simulants for chemical warfare agents. *J. Hazard. Mater.* **2011**, *194*, 85−91.

(8) Ghabili, K.; Agutter, P. S.; Ghanei, M.; Ansarin, K.; Panahi, Y.; Shoja, M. M. Sulfur mustard toxicity: history, chemistry, pharmacokinetics, and pharmacodynamics. *Crit. Rev. Toxicol.* **2011**, *41*, 384−403.

(9) Ashmore, M. H.; Nathanail, C. P. A critical evaluation of the implications for risk based land management of the environmental chemistry of Sulphur Mustard. *Environ. Int.* **2008**, *34*, 1192−1203.

(10) Cooley, K. A.; Pearl, T. P.; Varady, M. J.; Mantooth, B. A.; Willis, M. P. Direct measurement of chemical distributions in heterogeneous coatings. *ACS Appl. Mater. Interfaces* **2014**, *6*, 16289−16296.

(11) Willis, M. P.; Gordon, W.; Lalain, T.; Mantooth, B. Characterization of chemical agent transport in paints. *J. Hazard. Mater.* **2013**, *260*, 907−913.

(12) Liu, Y.; Du, X.; Wang, J.; Yin, Y.; Wang, B.; Zhao, S.; Li, N.; Li, C. High efficient detoxification of mustard gas surrogate based on nanofibrous fabric. *J. Hazard. Mater.* **2018**, *347*, 25−30.

(13) Gephart, R. T., 3rd; Coneski, P. N.; Wynne, J. H. Decontamination of chemical-warfare agent simulants by polymer surfaces doped with the singlet oxygen generator zinc octaphenoxyphthalocyanine. *ACS Appl. Mater. Interfaces* **2013**, *5*, 10191−10200.

(14) Ebrahim, A. M.; Plonka, A. M.; Tian, Y.; Senanayake, S. D.; Gordon, W. O.; Balboa, A.; Wang, H.; Collins-Wildman, D. L.; Hill, C. L.; Musaev, D. G.; et al. Multimodal Characterization of Materials and Decontamination Processes for Chemical Warfare Protection. *ACS Appl Mater. Interfaces* **2020**, *12*, 14721−14738.

(15) Sundarrajan, S.; Venkatesan, A.; Ramakrishna, S. Fabrication of Nanostructured Self-Detoxifying Nanofiber Membranes that Contain Active Polymeric Functional Groups. *Macromol. Rapid Commun.* **2009**, *30*, 1769−1774.

(16) Jung, K.-H.; Ji, L.; Pourdeyhimi, B.; Zhang, X. Structure−property relationships of polymer-filled nonwoven membranes for chemical protection applications. *J. Membr. Sci.* **2010**, *361*, 63−70.

(17) Browe, M. A.; Landers, J.; Tovar, T. M.; Mahle, J. J.; Balboa, A.; Gordon, W. O.; Fukuto, M.; Karwacki, C. J. Laponite-Incorporated UiO-66-NH_2-Polyethylene Oxide Composite Membranes for Protection against Chemical Warfare Agent Simulants. *ACS Appl. Mater. Interfaces* **2021**, *13*, 10500−10512.

(18) Lu, X.; Nguyen, V.; Zeng, X.; Elliott, B. J.; Gin, D. L. Selective rejection of a water-soluble nerve agent stimulant using a nanoporous lyotropic liquid crystal−butyl rubber vapor barrier material: Evidence for a molecular size-discrimination mechanism. *J. Membr. Sci.* **2008**, *318*, 397−404.

(19) Bhuiyan, M. A. R.; Wang, L.; Shaid, A.; Shanks, R. A.; Ding, J. Advances and applications of chemical protective clothing system. *J. Ind. Text.* **2019**, *49*, 97−138.

(20) Lee, S.; Obendorf, S. K. Barrier effectiveness and thermal comfort of protective clothing materials. *J. Text. Inst.* **2007**, *98*, 87−98.

(21) White, L. S. Development of large-scale applications in organic solvent nanofiltration and pervaporation for chemical and refining processes. *J. Membr. Sci.* **2006**, *286*, 26−35.

(22) Silva, P.; Han, S.; Livingston, A. G. Solvent transport in organic solvent nanofiltration membranes. *J. Membr. Sci.* **2005**, *262*, 49−59.

(23) Paul, D. Reformulation of the solution-diffusion theory of reverse osmosis. *J. Membr. Sci.* **2004**, *241*, 371−386.

(24) Ma, Y.; Kim, D.; Nutt, S. R. Chemical treatment for dissolution of amine-cured epoxies at atmospheric pressure. *Polym. Degrad. Stab.* **2017**, *146*, 240−249.
(25) Kuang, X.; Shi, Q.; Zhou, Y.; Zhao, Z.; Wang, T.; Qi, H. J. Dissolution of epoxy thermosets via mild alcoholysis: the mechanism and kinetics study. *RSC Adv.* **2018**, *8*, 1493−1502.
(26) Ha, S.; Lee, M.; Seo, H. O.; Song, S. G.; Kim, K. S.; Park, C. H.; Kim, I. H.; Kim, Y. D.; Song, C. Structural Effect of Thioureas on the Detection of Chemical Warfare Agent Simulants. *ACS Sens.* **2017**, *2*, 1146−1151.
(27) Picard, B.; Chataigner, I.; Maddaluno, J.; Legros, J. Introduction to chemical warfare agents, relevant simulants and modern neutralisation methods. *Org. Biomol. Chem.* **2019**, *17*, 6528−6537.
(28) Wang, F.; Liu, X. Upconversion multicolor fine-tuning: visible to near-infrared emission from lanthanide-doped NaYF4 nanoparticles. *J. Am. Chem. Soc.* **2008**, *130*, 5642−5643.
(29) Li, A.-F.; Wang, J.-H.; Wang, F.; Jiang, Y.-B. Anion complexation and sensing using modified urea and thiourea-based receptors. *Chem. Soc. Rev.* **2010**, *39*, 3729−3745.
(30) Zingaro, R. A.; Hedges, R. M. Phosphine oxide—halogen complexes: effect on p-o and p-s stretching frequencies1. *J. Phys. Chem. A* **1961**, *65*, 1132−1138.
(31) Zefirov, N.; Koz'min, A.; Kasumov, T.; Potekhin, K.; Sorokin, V.; Brel, V.; Abramkin, E.; Struchkov, Y. T.; Zhdankin, V.; Stang, P. Interaction of an allene with polyvalent iodine derivatives. Preparation, x-ray molecular structure, and some reactions of phenyl (2, 2-dimethyl-4-(diethylphosphono)-2, 5-dihydro-3-furyl) iodonium salts. *J. Org. Chem.* **1992**, *57*, 2433−2437.
(32) Gordon, W. O.; Peterson, G. W.; Durke, E. M. Reduced chemical warfare agent sorption in polyurethane-painted surfaces via plasma-enhanced chemical vapor deposition of perfluoroalkanes. *ACS Appl. Mater. Interfaces* **2015**, *7*, 6402−6405.
(33) Capricho, J. C.; Fox, B.; Hameed, N. Multifunctionality in Epoxy Resins. *Polymer Rev.* **2020**, *60*, 1−41.
(34) Yang, S.; Qu, J. Computing thermomechanical properties of crosslinked epoxy by molecular dynamic simulations. *Polymer* **2012**, *53*, 4806−4817.
(35) Shenogina, N. B.; Tsige, M.; Patnaik, S. S.; Mukhopadhyay, S. M. Molecular Modeling Approach to Prediction of Thermo-Mechanical Behavior of Thermoset Polymer Networks. *Macromolecules* **2012**, *45*, 5307−5315.
(36) Kaya, İ.; Gül, M.; Şenol, D. Synthesis and characterization of epoxy resins containing imine group and their curing processes with aromatic diamine. *J. Macromol. Sci., Part A* **2019**, *56*, 618−627.
(37) Li, J.; Wei, L.; Leng, W.; Hunt, J. F.; Cai, Z. Fabrication and characterization of cellulose nanofibrils/epoxy nanocomposite foam. *J. Mater. Sci.* **2018**, *53*, 4949−4960.
(38) Zaleski, R.; Krasucka, P.; Skrzypiec, K.; Goworek, J. Macro- and Nanoscopic Studies of Porous Polymer Swelling. *Macromolecules* **2017**, *50*, 5080−5089.
(39) Sienkiewicz, A.; Krasucka, P.; Charmas, B.; Stefaniak, W.; Goworek, J. Swelling effects in cross-linked polymers by thermogravimetry. *J. Therm. Anal. Calorim.* **2017**, *130*, 85−93.
(40) Barrie, J.; Nimis, A. S. A. *Permeability of Plastic Films and Coatings to Gases, Vapors, and Liquids*; Hopfenberg, H. B., Ed.; Plenum Press: New York, 1974.
(41) Rahman Bhuiyan, M. A.; Wang, L.; Shaid, A.; Shanks, R. A.; Ding, J. Polyurethane-aerogel incorporated coating on cotton fabric for chemical protection. *Prog. Org. Coat.* **2019**, *131*, 100−110.
(42) Narine, S. S.; Slavin, A. J. Use of the quartz crystal microbalance to measure the mass of submonolayer deposits: Measuring the stoichiometry of surface oxides. *J. Vac. Sci. Technol., A* **1998**, *16*, 1857−1862.
(43) Ramsdale-Capper, R.; Foreman, J. P. Internal antiplasticisation in highly crosslinked amine cured multifunctional epoxy resins. *Polymer* **2018**, *146*, 321−330.
(44) Levita, G.; De Petris, S.; Marchetti, A.; Lazzeri, A. Crosslink density and fracture toughness of epoxy resins. *J. Mater. Sci.* **1991**, *26*, 2348−2352.
(45) Gupta, V. B.; Drzal, L. T.; Lee, C. Y.-C.; Rich, M. J. The temperature-dependence of some mechanical properties of a cured epoxy resin system. *Polym. Eng. Sci.* **1985**, *25*, 812−823.
(46) Bouvet, G.; Dang, N.; Cohendoz, S.; Feaugas, X.; Mallarino, S.; Touzain, S. Impact of polar groups concentration and free volume on water sorption in model epoxy free films and coatings. *Prog. Org. Coat.* **2016**, *96*, 32−41.
(47) Jackson, M.; Kaushik, M.; Nazarenko, S.; Ward, S.; Maskell, R.; Wiggins, J. Effect of free volume hole-size on fluid ingress of glassy epoxy networks. *Polymer* **2011**, *52*, 4528−4535.
(48) Zhang, H. J.; Sellaiyan, S.; Sako, K.; Uedono, A.; Taniguchi, Y.; Hayashi, K. Effect of free-volume holes on static mechanical properties of epoxy resins studied by positron annihilation and PVT experiments. *Polymer* **2020**, *190*, No. 122225.
(49) Wang, Z.; Li, M.; Cai, Y.; Wang, J.; Wang, S. Novel CO_2 selectively permeating membranes containing PETEDA dendrimer. *J. Membr. Sci.* **2007**, *290*, 250−258.
(50) Tao, S. Positronium annihilation in molecular substances. *J. Chem. Phys.* **1972**, *56*, 5499−5510.
(51) Sauerbrey, G. Verwendung von Schwingquartzen zur Wagung dunner Schichten und zur Mikrowagung. *Z. Phys.* **1959**, *155*, 206−222.
(52) Höök, F.; Kasemo, B.; Nylander, T.; Fant, C.; Sott, K.; Elwing, H. Variations in Coupled Water, Viscoelastic Properties, and Film Thickness of a Mefp-1 Protein Film during Adsorption and Cross-Linking: A Quartz Crystal Microbalance with Dissipation Monitoring, Ellipsometry, and Surface Plasmon Resonance Study. *Anal. Chem.* **2001**, *73*, 5796−5804.

https://doi.org/10.1021/acsomega.2c00915
ACS Omega 2022, 7, 12354−12364